PFC/JA-86-22

# A New Look at Density Limits in Tokamaks

Gr eenwald, M.; Terry, J.; Wolfe, S.;
Ejima, S.*; Bell, M.†; Kaye, S.†; Neilson, G. H.‡

Plasma Fusion Center
Massachusetts Institute of Technology
Cambridge, MA 02139

*General Atomic Technologies
†Princeton Plasma Physics Laboratory
‡Oak Ridge National Laboratory

January 1988

This work was supported by the U. S. Department of Energy Contract No. DE-AC02-78ET51013. Reproduction, translation, publication, use and disposal, in whole or in part by or for the United States government is permitted.

# A New Look At Density Limits In Tokamaks

M. GREENWALD, J. TERRY, S. WOLFE
Plasma Fusion Center — M.I.T.

S. EJIMA *
General Atomic Technologies

M. BELL, S. KAYE
Princeton Plasma Physics Laboratory

G.H. NEILSON
Oak Ridge National Laboratory

## Abstract

While early work on the density limit in tokamaks from the ORMAK [1] and DITE [2,3] groups has held up well over the years, results from recent experiments and the requirements for extrapolation to future experiments have prompted a new look at this subject. There are many physical processes which limit attainable densities in tokamak plasmas. These processes include 1) radiation from low $Z$ impurities, convection, charge exchange and other losses at the plasma edge, 2) radiation from low or high $Z$ impurities in the plasma core, 3) deterioration of particle confinement in the plasma core, and 4) inadequate fueling, often exacerbated by strong pumping by walls, limiters, or divertors. Depending upon the circumstances, any of these processes may dominate and determine a density limit. In general, these mechanisms do not show the same dependence on plasma parameters. The multiplicity of processes which lead to density limits with a variety of scaling, has led to some confusion when comparing density limits from different machines. In this paper we attempt to sort out these various limits and extend the scaling

* Present address: Shin-Etsu Chemical Co., Ltd., 2-13-1, Isobe Annaka, Gunma, Japan

law for one of them to include the important effects of plasma shaping, namely that $\bar{n}_e = \kappa J$ where $n_e$ is the line average electron density ($10^{20} / m^3$), $\kappa$ is the plasma elongation and $J$ ( $MA / m^2$ ) is the average plasma current density, defined as the total current divided by the plasma cross sectional area. In a sense this is the most important density limit since, together with the $q$ limit, it yields the maximum operating density for a tokamak plasma. We show that this limit may be caused by a dramatic deterioration in core particle confinement occurring as the density limit boundary is approached. This mechanism can help explain the disruptions and marfes that are associated with the density limit.

## 1. Introduction

In exploring the operating regime of a tokamak, researchers have always found a limit in the maximum density that they could achieve. Attempts to raise the density beyond this limit result in a disruption of the discharge. The calue of the density limit is found to vary from machine to machine and with operating conditions in a systematic way. In this paper, we will consider several distinct limits. The first is the familiar Murakami limit with $n_e < B_T/R$ . The coefficient $m$ is not constant, but increases with input power and with plasma purity. A second and distinct limit is apparent when density is plotted against plasma current or (when these are normalized to toroidal field) as Murakami number, $n_e R/B$ vs$1/q$ . This is the DITE (or Hugill) plot and we will use the term "Hugill limit" to refer to density limits with $n_e \sim I_p$ [4]. Of course, experimental and theoretical investigations of these limits do not always yield such clear and simple scalings. We will suggest in a later section, that it might be more appropriate to distinguish between the limits by their underlying mechanism. That is, we would use "Murakami limit" to refer to operational limits imposed by plasma radiation and "Hugill limit" to refer to limits imposed by deterioration of particle confinement. For completeness we can include a third limit,

associated with an MHD threshold phenomenon that was observed by Granetz on Alcator C [5]. This behavior is not well understood, but leads to a density limit with $n_e \sim B^2$. Finally, there is a density limit which is imposed by the fueling process itself. Gas puffing alone is not always sufficient to reach the Murakami or Hugill limit. It is important to understand that all the density limits must be obeyed; the operating space of a tokamak will be limited by the minimum of the Murakami, Hugill, Granetz and fueling limits.

## 2. Scaling and Dependencies of the Density Limits

### 2.1. Murakami Limit

The Murakami limit was first proposed as an empirical scaling for the highest density achievable under any given discharge conditions. The $B/R$ scaling brought together results from a very wide range of machines working at density limits that varied over two orders of magnitude. The scaling was never exact of course, and as experimenters refined their techniques, particularly in the control of impurities, densities well above the original limit were subsequently reached. This has given rise to use of the Murakami number, which is simply the line averaged density divided by $B_T/R$. This allowed the comparison of density limits under different conditions, while normalizing out the strongest dependence. The Murakami number was seen to increase as $Z_{eff}$ approached 1 [6] and as additional heating, in the form of neutral beams, was applied [3,7]. This density limit has been attributed to a loss of balance between input and radiated power [1,8].

### 2.2. Hugill Limit

Additional insight into tokamak operating limits was obtained when plasma density was plotted against plasma current (or in their normalized form as Murakami number vs $1/q$ ) for a large number of discharges [4]. The earliest plots of this kind are from DITE for which data are shown in Fig. 1 [9]. Operational limits are determined from the boundaries of data on these plots. Three important features can be seen in this figure [10,11]. First,

there is a density limit proportional to plasma current; second, the proportionality constant between maximum density and plasma current is not increased with auxiliary heating; third, auxiliary heating allows the maximum density to be achieved at the higher plasma currents. We can understand the data in Figure 1 as resulting from the superposition of the limit on $q$ ( $q > 2$ ) and two distinct density limits; a "Hugill" limit with $n_{\max} \propto I_p$ independent of input power, and a Murakami limit with $n_{\max}$ independent of $I_p$ but strongly influenced by input power.

The operating space for all tokamaks shows these same general features. This is shown in schematic form in Fig. 2 in which the various limits we have identified are labeled. The use of the standard normalized axes, $I_p$ and the Murakami number allows direct comparison among machines. Figure 3 shows these DITE plots with data for several different tokamaks. For clarity, only the boundaries of experimentally accessible regions are drawn instead of including data points from individual discharges. If all machines showed the same Hugill density limit $n_{\max} = B/qR$ the lower boundary of each region should coincide. Although to lowest order the chosen normalization does bring together data from devices with widely varying parameters, it is clear from this figure that substantial systematic differences between the devices remain. In particular we note that machines capable of producing strongly shaped plasmas, reach the highest $n_e/I_p$ . Of course, differences between the density limits on various machines might be due to differences in experimental technique, or to differences, from machine to machine, in the physics that sets the density limit. Neither of these alternatives is very attractive since they do not help us understand the physics of the limit nor do they allow us to extrapolate to density limits on future machines. Fortunately, if past experience is a guide, the explanation is that we simply do not have quite the right scaling expression.

Under the assumption that a common cause is responsible for setting this density limit on all machines, we can look for a scaling that can bring all the data into line. We can begin by noting that the equation $n_{\max} \sim \frac{B}{qR}$ is close, within a factor of two, of the expression we are seeking and thus a first approximation, $n \sim \frac{I_p}{a^2}$ . It should be pointed out that there is no consensus in the literature on which "form" of $q$ to use in plotting the density limit. Various approximations of $q_\psi$ and $q_{cylindrical}$ are used along with expressions like $q = \frac{5a^2 B}{IR}$ , that are only correct for circular machines and in the limit of high aspect ratio and low beta. If the plasma safety factor is important in the physics of the density limit rather than simply a convenient normalization of the plasma current, then we would expect $q_\psi$ to be the correct term to use. In Fig. 3 we have plotted data from Alcator C, DIII, and PBX against $q_\psi$ . This is not the scaling we are looking for; $q_\psi$ does not seem to be an important quantity with respect to the density limit.

By fitting the available data to very simple combinations of the machine parameters, we arrive at an expression that does bring data from the various machines together,

$$\bar{n} = \kappa \bar{J}$$

measured in $10^{20}/m^3$ , $\kappa$ is the plasma elongation, and $\bar{J}$ is the average plasma density, $I_p$ area measured in $MA/m^2$ . Figs 4a-d are modified Hugill plots for several machines showing the results of this scaling. They should be compared with figure 3. For elliptical machines, this scaling for the density limit can be written as $\bar{n}_{\max} = \frac{I_p}{\pi a^2}$ and for high aspect ratio, low beta, circular machines it can be written as $\frac{5}{\pi} \times \frac{B}{qR}$ . A few comments on the simplicity of equation 1 are in order. It is almost certain that the dependence on plasma size and elongation given by equation 1 are not exact, that additional dependencies on shape parameters exist. By its nature, the density limit boundary can

only be approximately defined. As the limit is approached, the plasma becomes increasingly susceptible to disruption and data become sparser, so that quite aside from ordinary errors in the measurement of experimental quantities, the definition of the boundary is somewhat subjective. Data that would allow more precise calculation of parametric dependencies are not easily obtained.

### 2.3 Fueling Related Limits

The importance of an adequate fuel source in reaching a density limit seems obvious but is often overlooked (consider in fact, the density "limits" that were observed before the technique of gas puffing was introduced.) As machines have become larger and denser, the mean free path for low energy neutrals has become smaller when compared to minor radius, and gas fueling has become less effective. This can be clearly seen in DITE plots for JET and TFTR where ohmic, gas fueled plasmas are compared with those fueled by pellet injection (Fig 5) [12,13]. Injection of high speed frozen hydrogen pellets introduces fuel directly into the plasma core, avoiding the limitations associated with gas puffing. The same effect can be achieved by fueling with neutral beams (Figs 6 [13]) which can yield plasmas at the same densities as those with pellet fueling and ohmic heating. The higher densities seen in this case have been attributed to the additional power that is added along with the particles [13]. However if we consider JET discharges with RF heating that adds no particles, these yield the same low densities as gas fueled ohmic plasmas. This was explained as the effect of additional impurities introduced by the RF heating. If this were the case, it would be expected that plasmas with RF and NBI would not reach the same densities as NBI alone since the RF would add impurities in either case. This is contradicted by the data, which shows the RF + NBI plasmas achieving the same densities as NBI or pellet fueled discharges. Another clear example of a fueling related density limit can be seen in data from Alcator C (Fig. 7). The highest densities obtainable for the machine configured with carbon limiters and gas fueling are about half of those found with

molybdenum limiters. That this difference is due to deficient fueling can be seen by observing that pellet fueled carbon limiter plasmas have the same density limit as those with molybdenum. Presumably the strong pumping effect of carbon accounts for the difference seen with gas fueling [14]. A similar effect probably accounts for the higher densities reported on TFTR with helium gas when compared to hydrogen or deuterium [15, 16]. Limiters, walls, and divertors can all compete effectively with the plasma for hydrogen fuel at the plasma edge.

### 2.4 Granetz Limit

For completeness we will identify an additional density limit associated with an MHD threshold phenomenon. On Alcator C, low $m$ coherent MHD oscillations were observed when the line averaged density was raised above $n_c \sim B^2$ [5] Fig. 8. This limit did not scale with plasma current over a wide range $2.7 < q < 4.7$ MHD amplitude increased rapidly for $n > n_c$ until, at densities about 40% above the MHD threshold, a disruptive density limit was reached. This behavior has not been seen on other machines, however this may be explained by later work that showed a significant size scaling with $n_c \sim a^2$ or higher [12]. It is interesting to note that a strong degradation in impurity confinement was correlated with the rise in MHD activity $1/\tau_I \sim (n - n_c)^4$ [18].

## 3. Physics of the Density Limits

The operating space for a tokamak is bounded in most cases by the occurrence of major disruptions. It would be wrong of course, to look for the cause of operational limits solely in the MHD equations (where electron density does not enter explicitly). It may be useful to think of the destruction of the MHD equilibrium as the final (fatal) symptom of some other underlying malady. For some time [1,8], excessive radiation has been identified as the cause behind the density limit disruption. This is logical since radiated power increases with density but input power does not. As radiation losses increase, the

plasma temperature profile and plasma current channel both shrink leading ultimately to the loss of MHD stability. Several authors have derived expressions for a density limit determined by this mechanism that are in rough agreement with experimental measurements. Gibson [19], Ohyabu [20], Ashby [21], Wesson [22] and Roberts [23] have calculated the conditions required for thermal instability and MHD collapse due to impurities radiating in thin shells at the plasma boundary. Ashby and Hughs find for example,

$$n_{\max} \sim \frac{B}{qR}\left(\frac{Z_{eff}}{Z_{eff}^{-1}}\right)^{1/2} \frac{1}{\overline{T}_e^{\,1/2}} \qquad (2)$$

Perkins and Hulse [24] calculate a density limit by requiring power balance between input and radiated power in the plasma core. The expressions they derive can be written as

$$n_{\max} \sim \frac{1}{(Z_{eff}^{-1})^{1/2}} \frac{B}{R} \qquad (3)$$

which agrees with Murakami's scaling and mechanism. Observations would appear to support these models; the highest densities are achieved with auxiliary heating and in clean discharges (low $Z_{eff}$).

Closer inspection of the data reveals some problems with this picture. While the higher densities are reached at higher input power, the slope of $n_{\max}$ vs $I_p$ is not much affected (Figs 1, 4), at least for plasmas with adequate fueling (see discussion of fueling limits). This was recognized by Hugill [10,11], who suggested that radiation may not be responsible for this density limit. For relatively clean plasmas, this boundary is not dependent on impurity level either. In Fig. 9, the ratio of measured density to the density limit, $\overline{n} = \kappa J$ is plotted against $Z_{eff}$ and shows that the density limit is accessible for $Z_{eff}$ up to 1.5 and perhaps as high as $Z_{eff} = 2$. Data from ISX-B (Fig. 10) show a similar result

when discharges from gettered and ungettered vacuum chambers are compared. In contrast, the theoretical treatments divege as $Z_{eff} \rightarrow 1$ limited only by hydrogen bremsstrahlung, which is overwhelmed by impurity radiation at $Z_{eff}$ in the outer regions of the plasma at $Z_{eff}$ only slightly above 1.

Results from a series of pellet fueling experiments on Alcator C [25] suggest an alternate approach to this problem. In these experiments, single pellets were injected into plasmas with relatively low plasma current. The density increased very quickly at the time of injection, .27 sec, for all discharges and the rate of density decay was monitored (Fig. 11). As the plasma current was lowered, shot to shot, the decay time decreased dramatically. Calculations summarized in table 1 show that the density limit, established with gas fueling, was greatly exceeded. These discharges did not disrupt however, but simply "shed" particles in excess of the limit. The density decay time is not the same as particle confinement time but is closely related. At steady state the particle confinement is given by the ratio of density to source, however in those cases where the time derivative dominates the source term, the density decay time will equal the particle confinement time, $\tau_p$ . Unlike the conventionally defined global $\tau_p$ which is dominated by the large particle fluxes in the plasmas edge, this confinement time is characteristic of the plasma core. It is worth pointing out that no decline in energy confinement accompanied the drop in particle confinement except the convective loss directly associated with the density decay. Figure 12 shows the results when the density decay time is plotted vs $J/n$ for a larger collection of shots. The precipitous drop in particle confinement occurs in the neighborhood of the previously derived density limit. The same data is plotted in another form in Fig. 13, which is a conventional DITE plot where data from pellet shots with fast decay rates are shown as solid circles. Table 1 tabulates data from Fig. 11. Shown for each shot, are the plasma current, the ratio of the maximum density for each discharge to the density limit, the

calculated density limit, $\kappa \bar{J}$ and the density decay time from a fit to the curve (which is necessarily taken after the peak of the density).

**Table I**

| $I_p$ | $n_{peak}/\kappa \bar{J}$ | $n_{limit}$ ( $cm^{-3}$ ) | $\tau_n$ ($msec$) |
|---|---|---|---|
| 370$kA$ | 1.2 | $4.3 \times 10^{14}$ | 51 |
| 220$kA$ | 2.0 | $2.6 \times 10^{14}$ | 19 |
| 220$kA$ | 2.4 | $2.1 \times 10^{14}$ | 7 |

If the deterioration of particle confinement described above is a general feature of tokamak discharges it could be the prime mover behind the density limit. (At the least it allows us to push the chain of cause and effect back one more step. We need to add here that while this explanation may explain various aspects of the density limit, the authors offer no insight into the physical mechanism that might lie behind the transport deterioration.) This does not mean that radiation does not play an important role in the $n - I_p$ limit. With deteriorating confinement, it takes an ever larger source of fuel for each incremental increase in density as a machine is pushed towards the limit. This will result in higher edge densities, more radiation, and lower edge temperatures. Ultimately the current profile and MHD stability are sufficiently altered to cause a major disruption. Of course, even in the absence of radiation, convective, ionization, and charge exchange losses would eventually lead to the same result. (Allen [26] has reported that increased energy transport in the plasma periphery plays a role in density limit disruptions in the DITE tokamak.) With pellet fueling, it is possible to raise the central density without affecting the edge, thus the limit can be exceeded without disruption, revealing the transport deterioration by itself.

We would not want to claim that deterioration of particle confinement is the only mechanism for density limit disruptions. We have already seen that the balance between radiation and input power can determine how much of the $n - I_p$ curve is accessible. For sufficiently dirty plasmas, radiation alone can cause the operating range to contract from

all the operational boundaries [3,24]. We have previously distinguished between two density limits based on their scaling; perhaps it would be better to make the distinction based on mechanism. The Murakami limit would apply to the limit, whatever its exact scaling on $B_T$ , $I_p$ and size, where radiation was the principle cause, and the Hugill limit would apply to the limit based on deterioration of particle confinement. The mechanism that we are proposing allows us to connect the Hugill limit to the fueling limit as well. Since the plasma density results from the balance of source and loss, deterioration of particle confinement with $n/J$ can act in tandem with processes which reduce the particle source. This may also explain the observation that fueling limits often show the $n_e - I_p$ scaling.

The same mechanism we propose to explain the Hugill density limit may underlie the appearance of Marfes [28]. Marfes are bands of very high density, low temperature, poloidally asymmetric plasma that appear at the periphery of tokamak plasmas as the density limit is approached. Typically, Marfes occur at 60 - 80% of the density limit. They are believed to be a thermal condensation phenomenon [19, 29] localized by neoclassical flows in the edge plasma. If our new understanding of the density limit is correct, Marfes can be thought of as the first symptom of the deteriorating particle confinement. As particle confinement falls, with energy confinement fixed, the ratio of power flux to particle flux at the edge falls as well. This means there will be more particles at the edge and they will have lower average energy. These are just the right starting conditions for a thermal condensation. Of course details of the edge profiles, impurity content, and plasma flows will all affect the onset and characteristics of the Marfe.

## 4. Summary

We have distinguished between several different density limits. The first, the Murakami limit, is caused by an unfavorable balance between input and radiated power and scales as $n - B_T/R$ for ohmically heated plasmas. The same physics could lead to

dependence on plasma current at lower densities. It is strongly affected by plasma purity and of course by auxiliary or alpha heating. With sufficient input power the Murakami limit can be pushed to very high values. The second, which we have called the Hugill limit, depends principally on current density and plasma cross section and may be due to a degradation in particle confinement time as the density limit is approached. Scaling this limit as $\bar{n} = \kappa J$ brings much of the available data base into line. In a sense it is the most important density limit, since together with the disruptive limit on plasma current ( $q_\Psi > 2$ ), it defines the operating space for a tokamak and will yield the highest steady state density achievable on a given machine. In the case of large and/or high density tokamaks or in the presence of processes which compete with the plasma for fuel, this limit may be difficult to reach. With particle confinement declining with $n/J$, any decrease in particle source will result in lower densities. Inadequate fueling represents a third limit on density. All of the above limits must be obeyed; the operating space of a tokamak will be limited by the minimum of the Murakami, Hugill, and fueling limits.

**Acknowledgements**

The authors wish to thank the Alcator C, Doublet, ISX and PDX/PBX experimental groups for contributing data for this study. They also thank John Sheffield and Ron Stambaugh and other members of the Ignition Physics Study Group (IPSG) for the initial impetus and for many useful discussions.

## References


[1] MURAKAMI, M., CALLEN, J.D., BERRY, L.A. Nucl. Fus.,**16**, 347 (1976)

[2] PAUL, J.W.M., AXON, K.B., BURT, J., et al., Plasma Physics and Controlled Nuclear Fusion Research (Proc. 6th Int. Conf. Berchtesgaden, 1976) Vol. II, 269, IAEA, Vienna, (1977)

[3] AXON, K.B., BAXTER, G.A., BURT, J., et al., Plasma Physics and Controlled Nuclear Fusion Research (Proc. 7th Conf. Innsbruck, 1978), Vol I, 51, IAEA, Vienna, (1979)

[4] P.E. Stott, J. Hugill, S.J. Fielding, et al., Proceedings of the 8th European Conference on Controlled Fusion and Plasma Physics, Prague 1979, Vol 1, pg 151

[5] GRANETZ, R., Phys. Rev. Lett. 49, 658, (1982)

[6] FIELDING, S.J., HUGILL, J., McCRACKEN, G.M., et al., Nucl. Fus. **17**, 1382 (1977)

[7] BERRY, L.A., BUSH, C.E., CALLEN, J.D., et al., Plasma Physics and Controlled Nuclear Fusion Research (Proc 6th Int. Conf. Berchtesgaden, 1976) Vol I, 49, IAEA Vienna, (1977)

[8] VERSHKOV, V.A., MIRNOV, S.V., Nucl. Fus. **14**, 383, (1972)

[9] AXON, K.B., CLARK, W.H.M., et al., Plasma Physics and Controlled Nuclear Fusion Research (Proc. 8th Int. Conf. Brussels, 1980) Vol 1., 413, IAEA Vienna (1981)

[10] HUGILL, J., Proceedings of the 2nd Joint Grenoble-Varenna International Symposium on Heating in Toroidal Plasmas, Como 1980, pg 775

[11] HUGILL, J., LOMAS, P.J., WOOTTON, A.J., et al., " High Density Operation in DITE with Neutral Beam Injection", CLM-R239, (1983)

[12] SCHMIDT, G.L., MILORA, S.L., ARUNASALEM, V., et al., Plasma Physics and Controlled Nuclear Fusion Research (Proc. 11th Int. Conf. Kyoto, 1986) Vol I, 171, IAEA Vienna, (1987)

[13] JET, Plasma Physics and Controlled Fusion, Vol. 29, No. 10A, 1219, (1987)

[14] WILSON, K.L., and HSU, W.L., Journal of Nuclear Materials 145-147 (1987) p. 121.

[15] DYLLA, H.F., LAMARCHE, P.H., ULRICKSON, M., Nucl. Fus. **27**, 1221 (1987).

[16] BELL, M., ARUNASALEM, V., BITTER, M., et al., Plasma Physics and Controlled Fusion, Vol 28, No. 9a, 1329, (1986)

[17] FIORE, C., Private Communication (1986).

[18] MARMAR, E.S., RICE, J.E., TERRY, J.L., SEQUIN, F.H., Nucl. Fus. **22**, 1567, (1982

[19] GIBSON, A., Nucl. Fus. **16**, 546, (1976)

[20] OHYABU, N., Nucl. Fus. **19**, 1491, (1979)

[21] ASHBY, D.E.T.F., HUGHES, M.H., Nucl. Fus. **21**, 911, (1981)

[22] WESSON, J., GOWERS, C., HAN, W., et al., eps Budapest p147 1985

[23] ROBERTS, D.E., Nucl. Fus. **23**, 311 (1983).

[24] PERKINS, F.W., HULSE, R.A., Phys. Fluids 28, 1837, (1985)

[25] GREENWALD, M., BESEN, M., CAMACHO, F., et al., Plasma Physics and Controlled Nuclear Fusion Research (Proc. 11th Int. Conf. Kyoto 1986) Vol I, 139, IAEA, Vienna, (1987)

[26] ALLEN, J., AUSTIN, G.E., AXON, K.B., et al., Plasma Physics and Controlled Nuclear Fusion Research (Proc. 11th Int. Conf. Kyoto 1986) Vol I, 227, IAEA Vienna, (1987)

[27] PFEIFFER, W., and WALTZ, R.E., Nucl. Fus. **19**, 51 (1979)

[28] LIPSCHULTZ, B., LABOMBARD, B., MARMAR, E.S., et al., Nucl. Fus. **24**, 977 (1984)

[29] DRAKE, J., Phys. Fluids 30, 8, (1987)

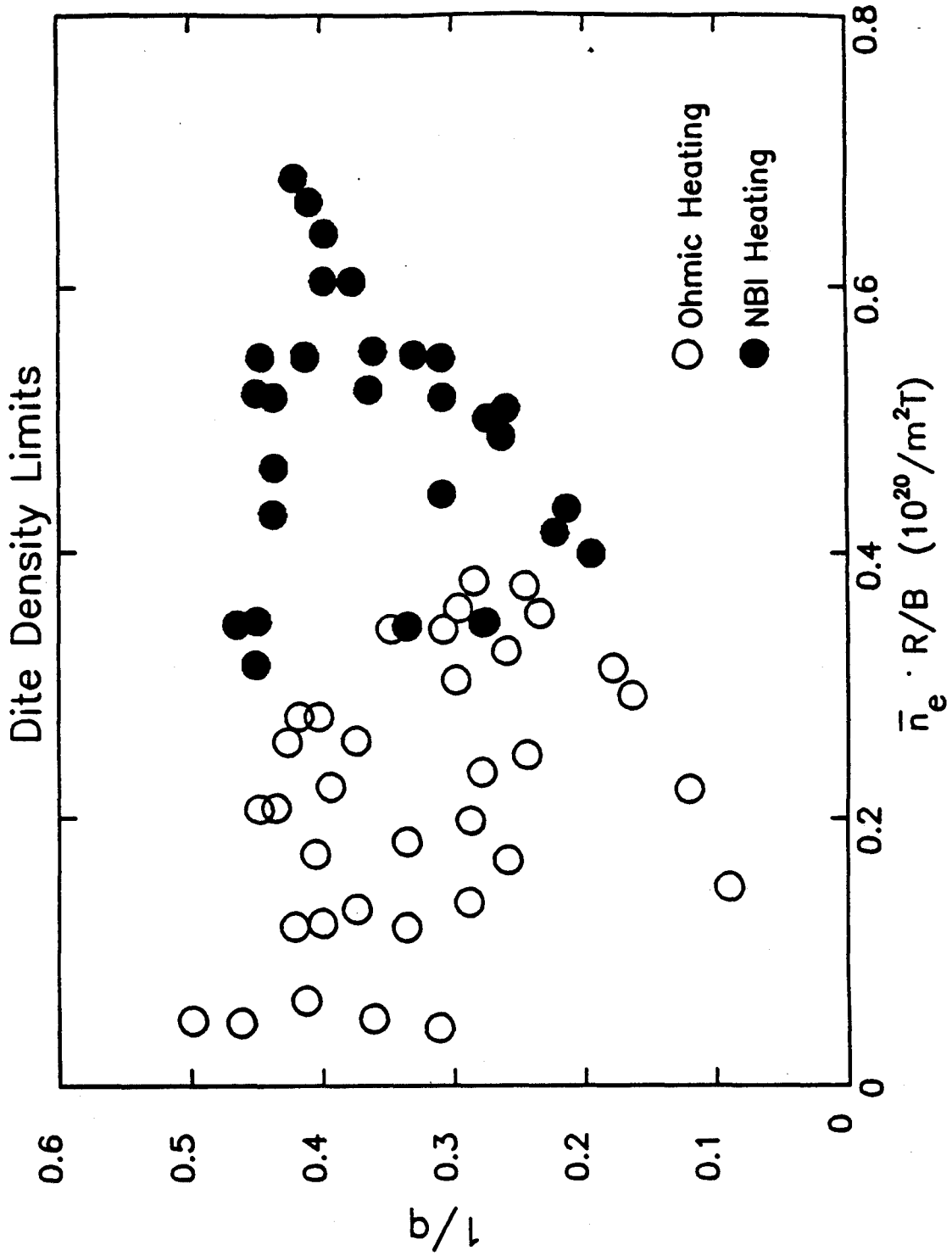


**Figure 1.** DITE (or Hugill) plot for DITE plasmas [9]. Each plotted point represents an individual discharge and the operating range is given by the envelope of these points.

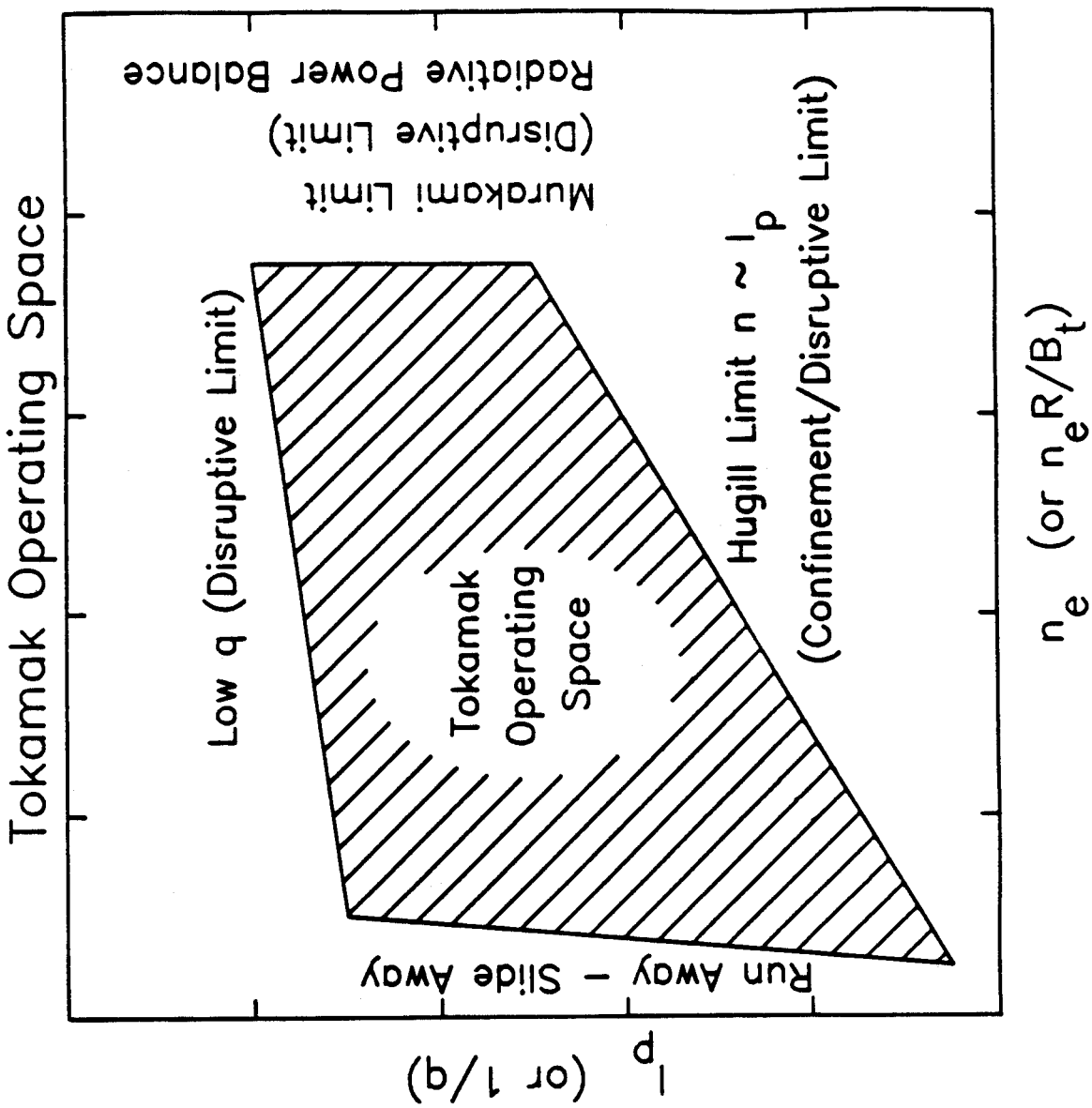


**Figure 2.** Schematic for DITE plot with operating limits identified.

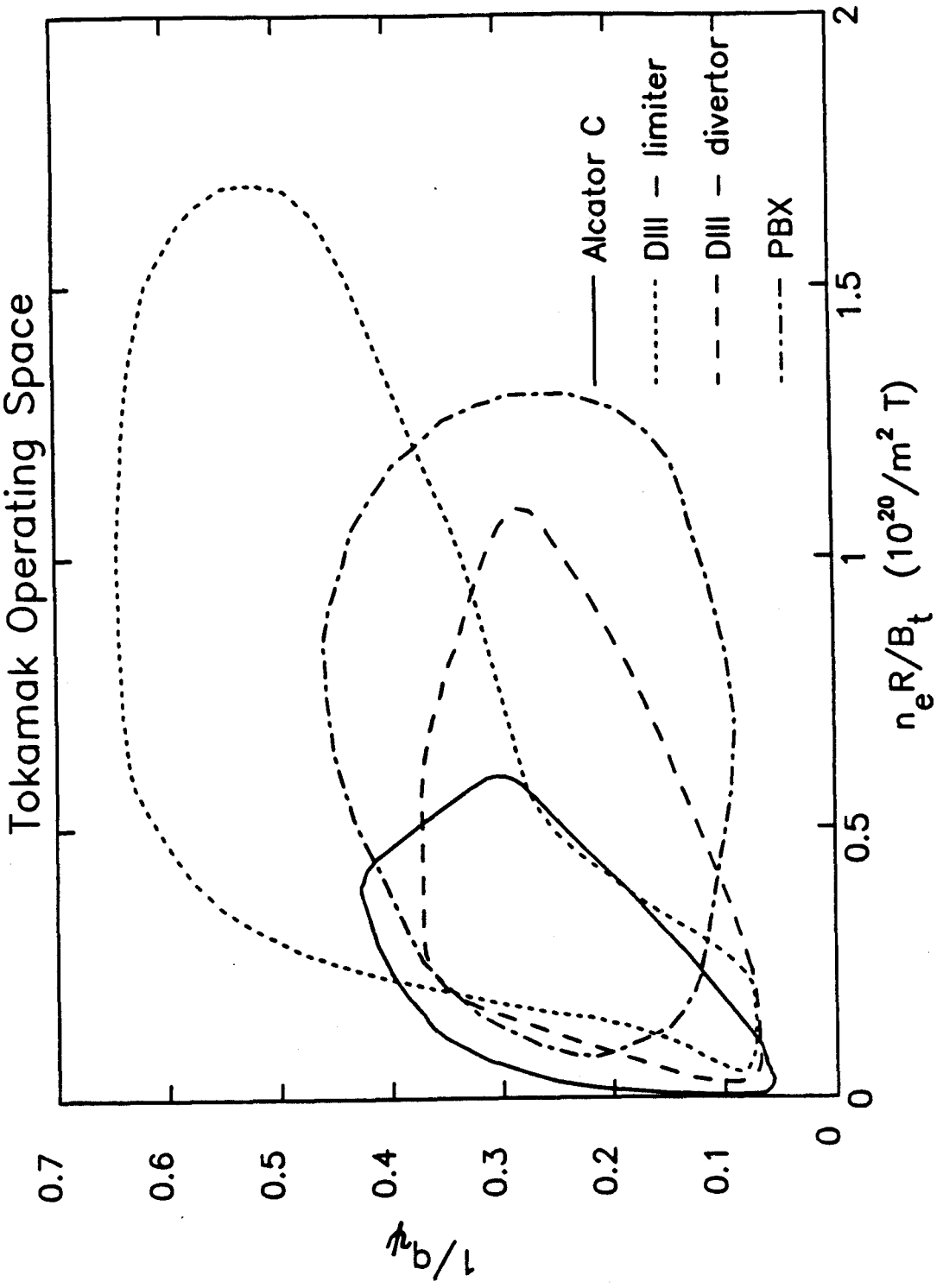


**Figure 3.** DITE plot comparing data from Alcator C, DIII and PBX. The abscissa is explicitly $1/q_\Psi$ .

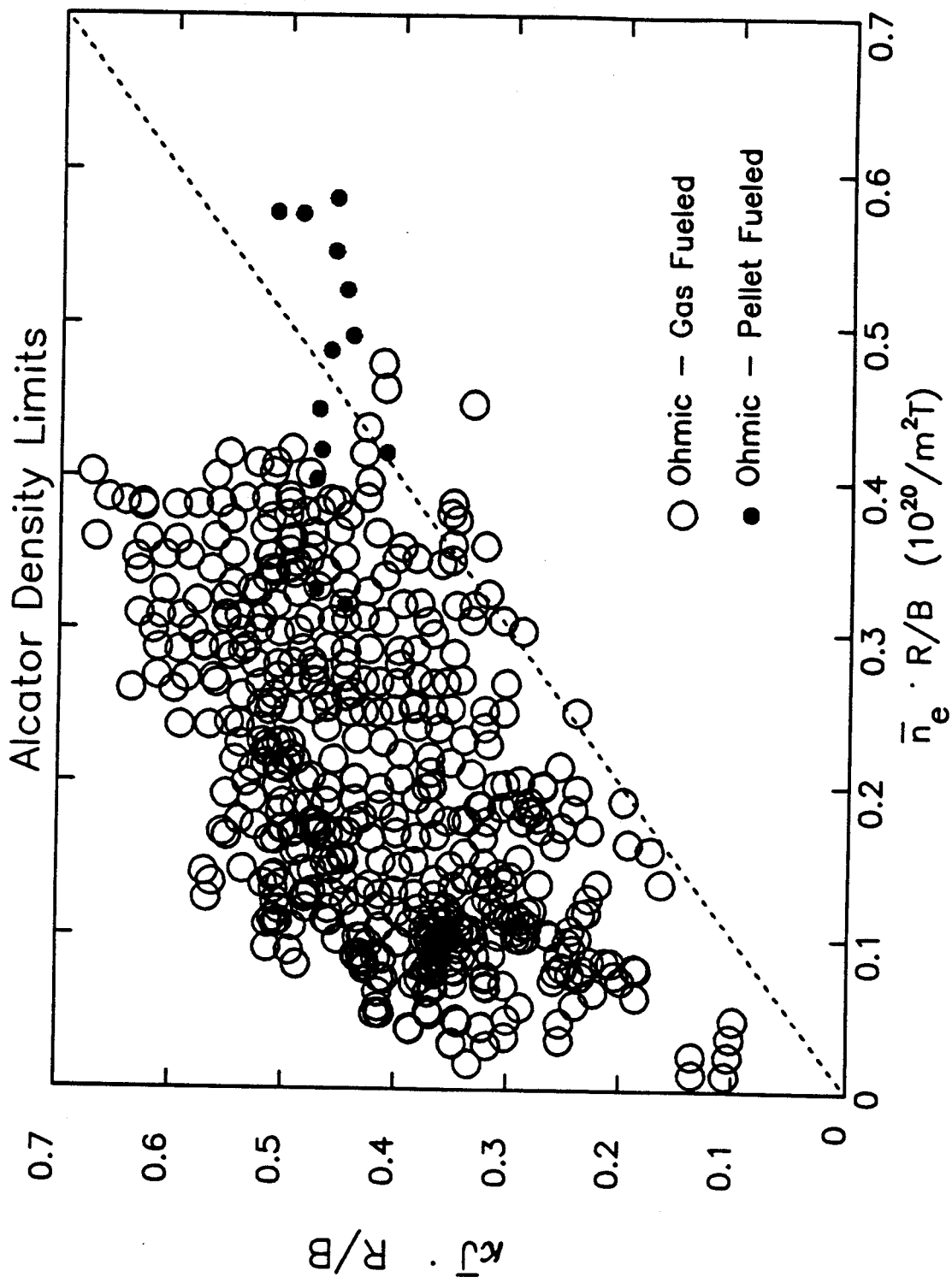


**Figure 4a.** Alcator C

Plots of density versus the scaling parameter $\kappa J$ for the same data as figure 3

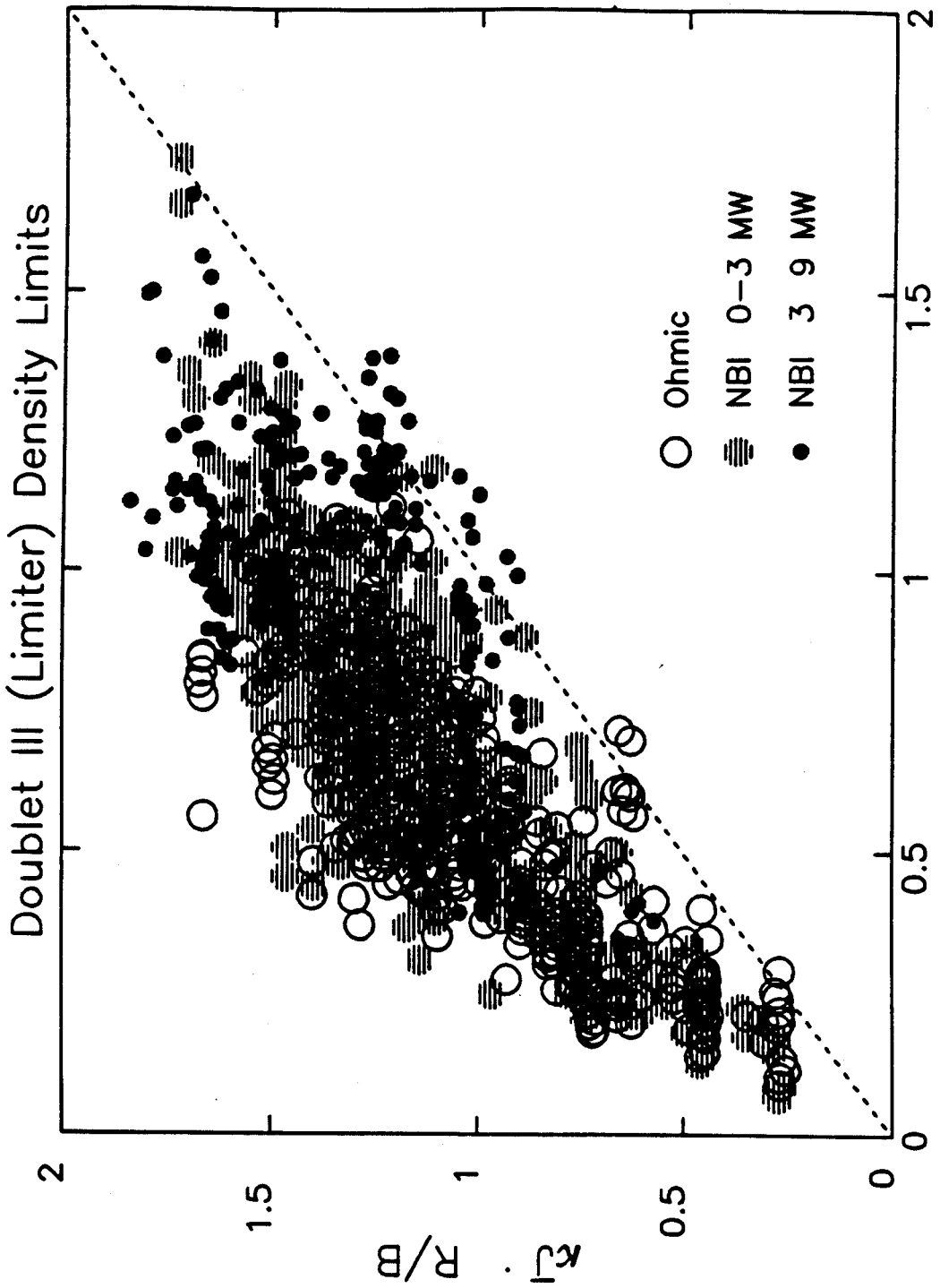


**Figure 4b.** DIII limiter

Plots of density versus the scaling parameter $\kappa J$ for the same data as figure 3

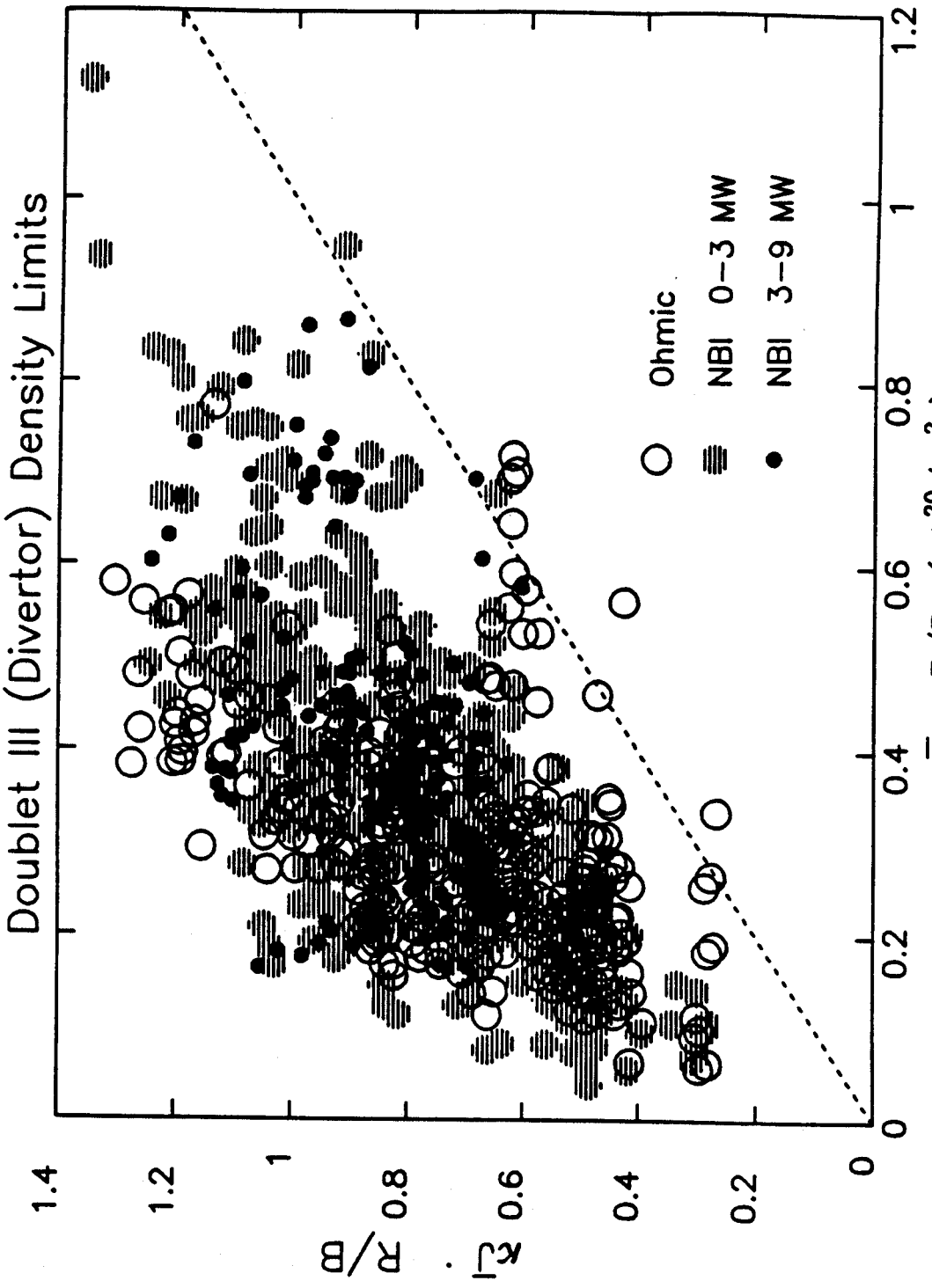


**Figure 4c.** DIII divertor

Plots of density versus the scaling parameter $\kappa_J$ for the same data as figure 3

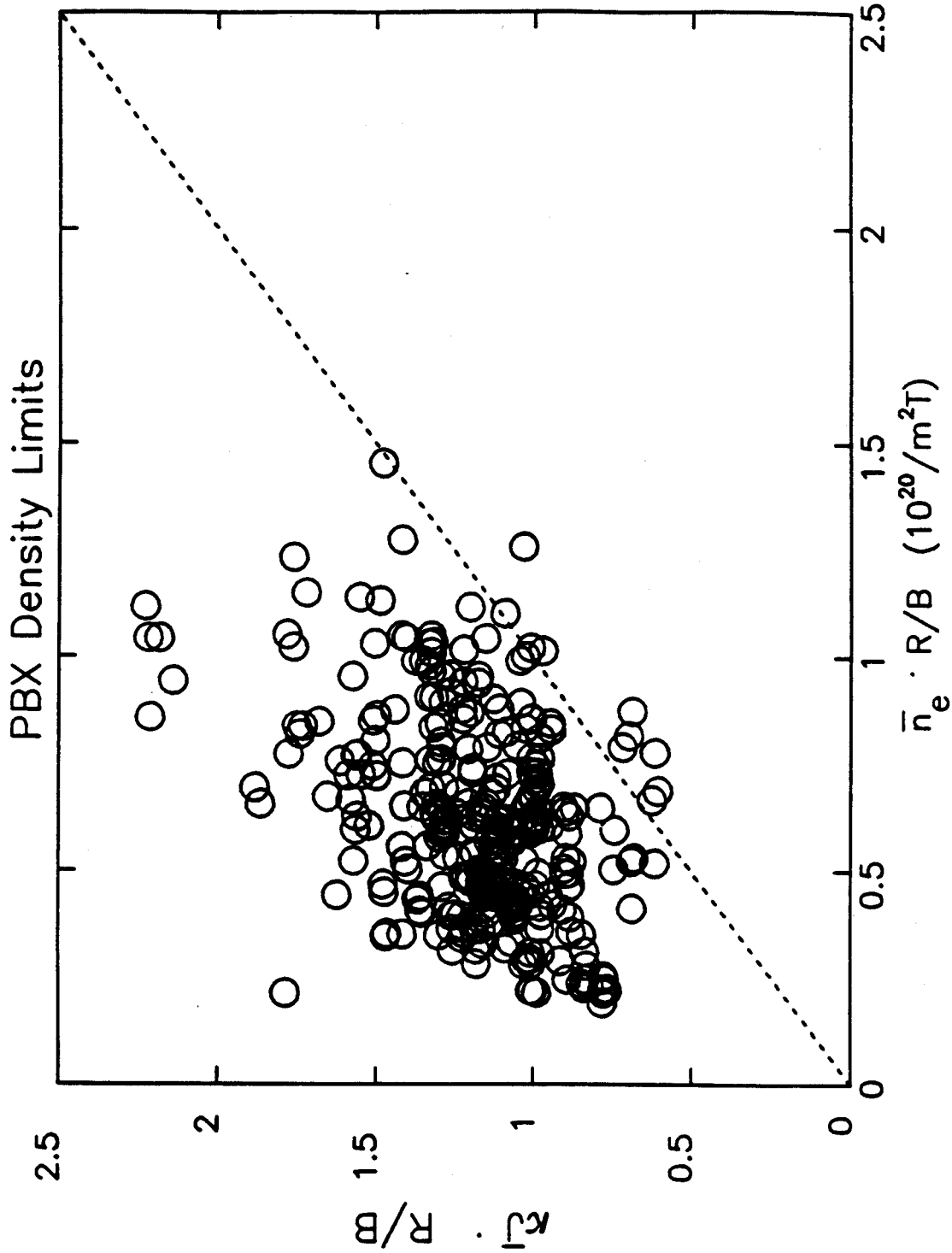


**Figure 4d.** PBX

Plots of density versus the scaling parameter $\kappa J$ for the same data as figure 3

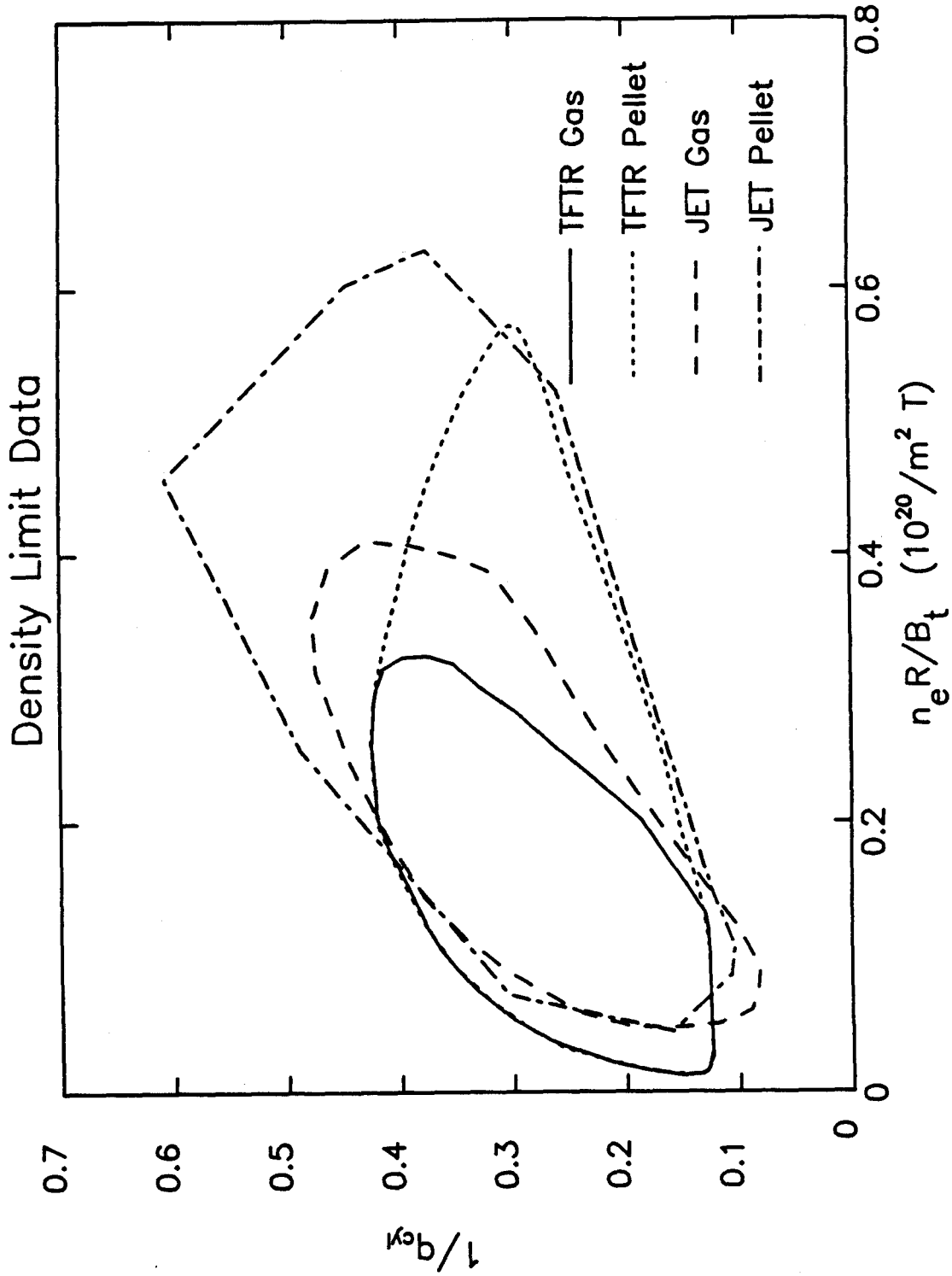


**Figure 5.** A comparison of operating space for gas and pellet fueled discharges for two l large tokamaks, JET and TFTR. The limits established with gas fueling are easily overcome with an adequate fueling technique.

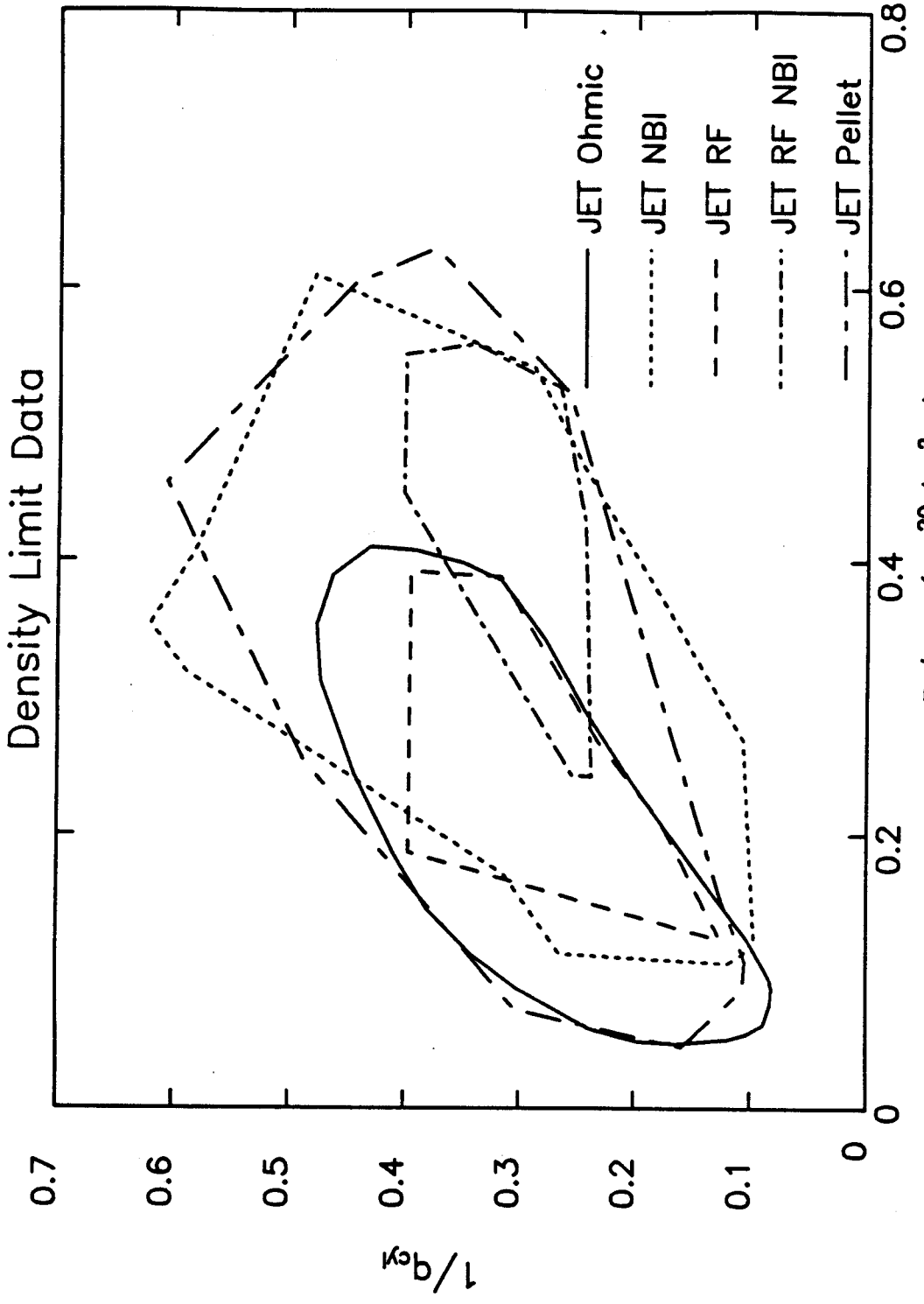


**Figure 6.** A comparison of operating space for JET discharges with Ohmic, NBI, ICRF, and NBI + ICRF heating.

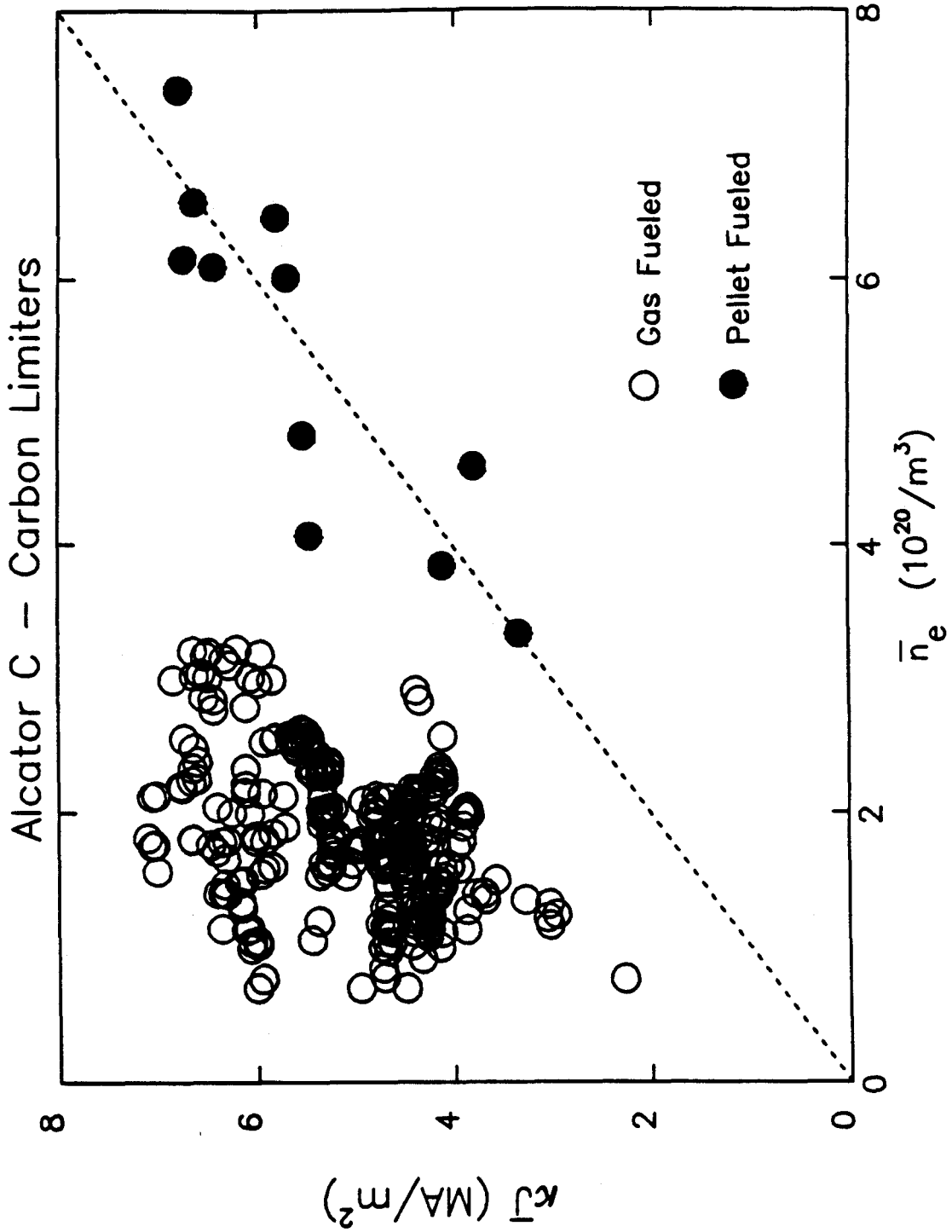


**Figure 7.** Alcator C data taken with carbon limiters. The solid points are for discharges with pellet fueling and the machine configured with carbon limiters. The dashed curve is for gas fueled plasmas and molybdenum limiters.

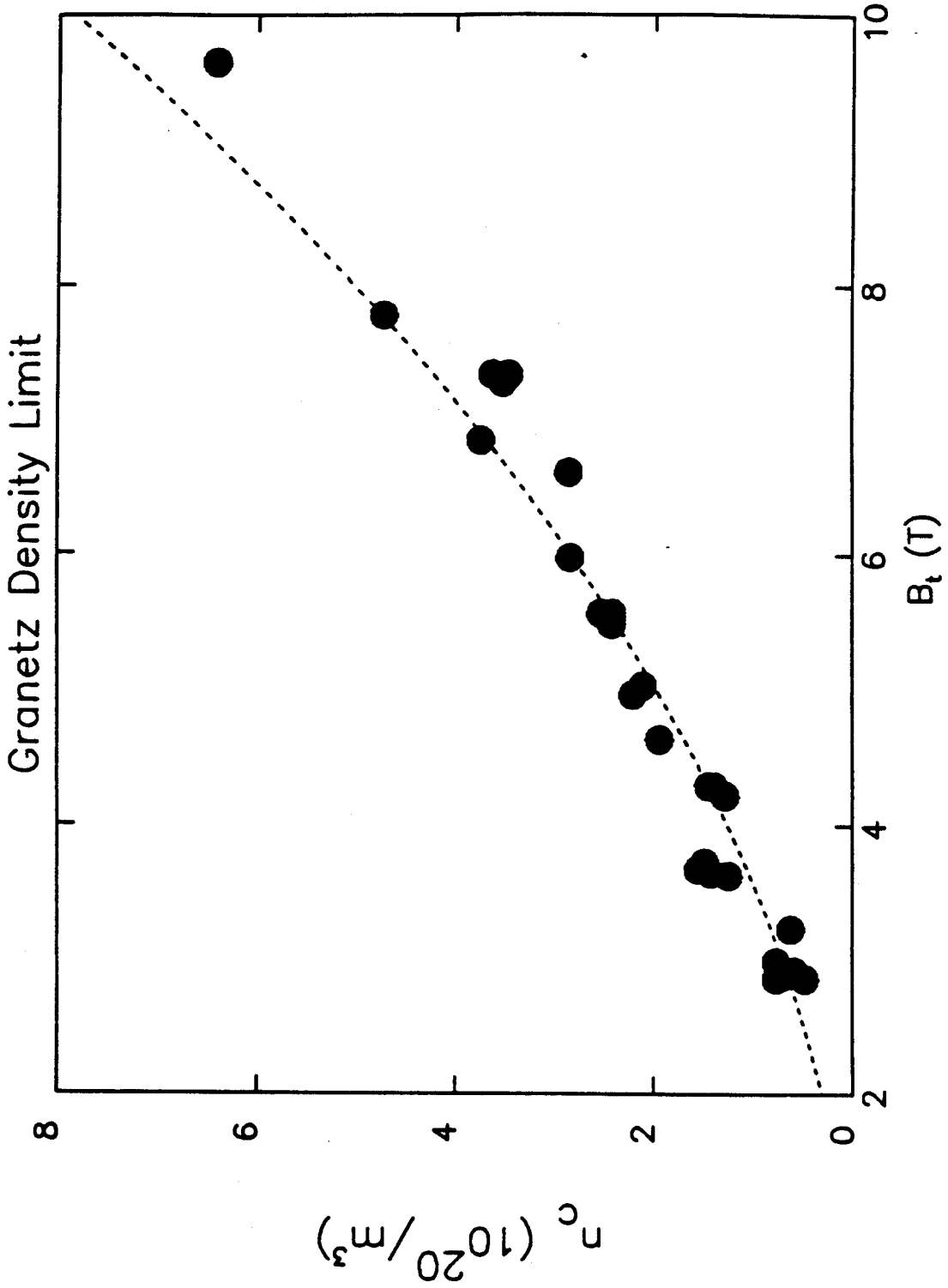


**Figure 8.** The Granetz threshold for MHD activity (Alcator C). A density limit is found about 40% above the MHD threshold.

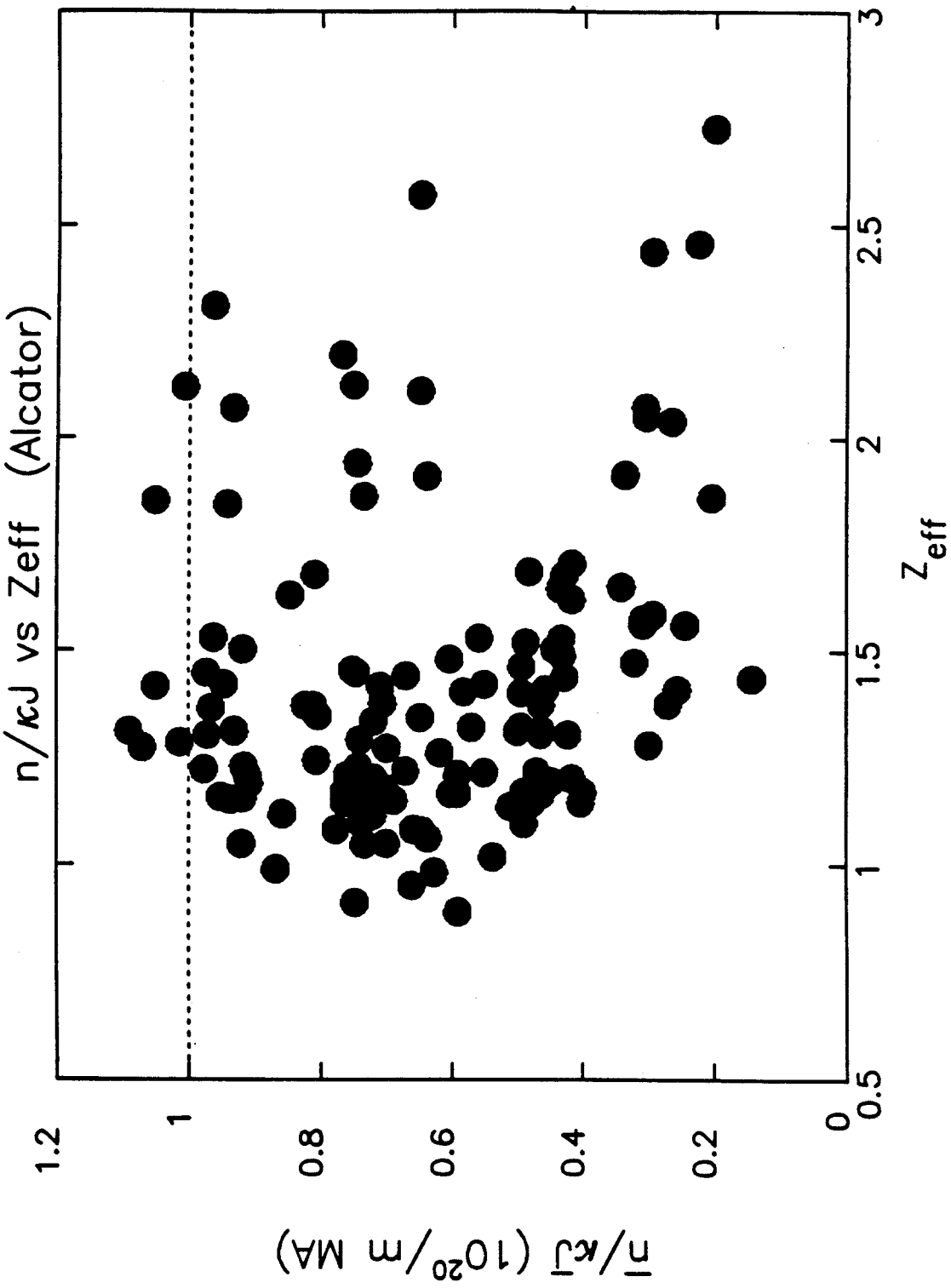


**Figure 9.** Density (normalized to $\kappa J$) vs $Z_{eff}$ . The dashed curve which represents the scaled limit, $n = \kappa J$ can be reached for plasmas with $Z_{eff}$ substantially above 1 (Alcator C).

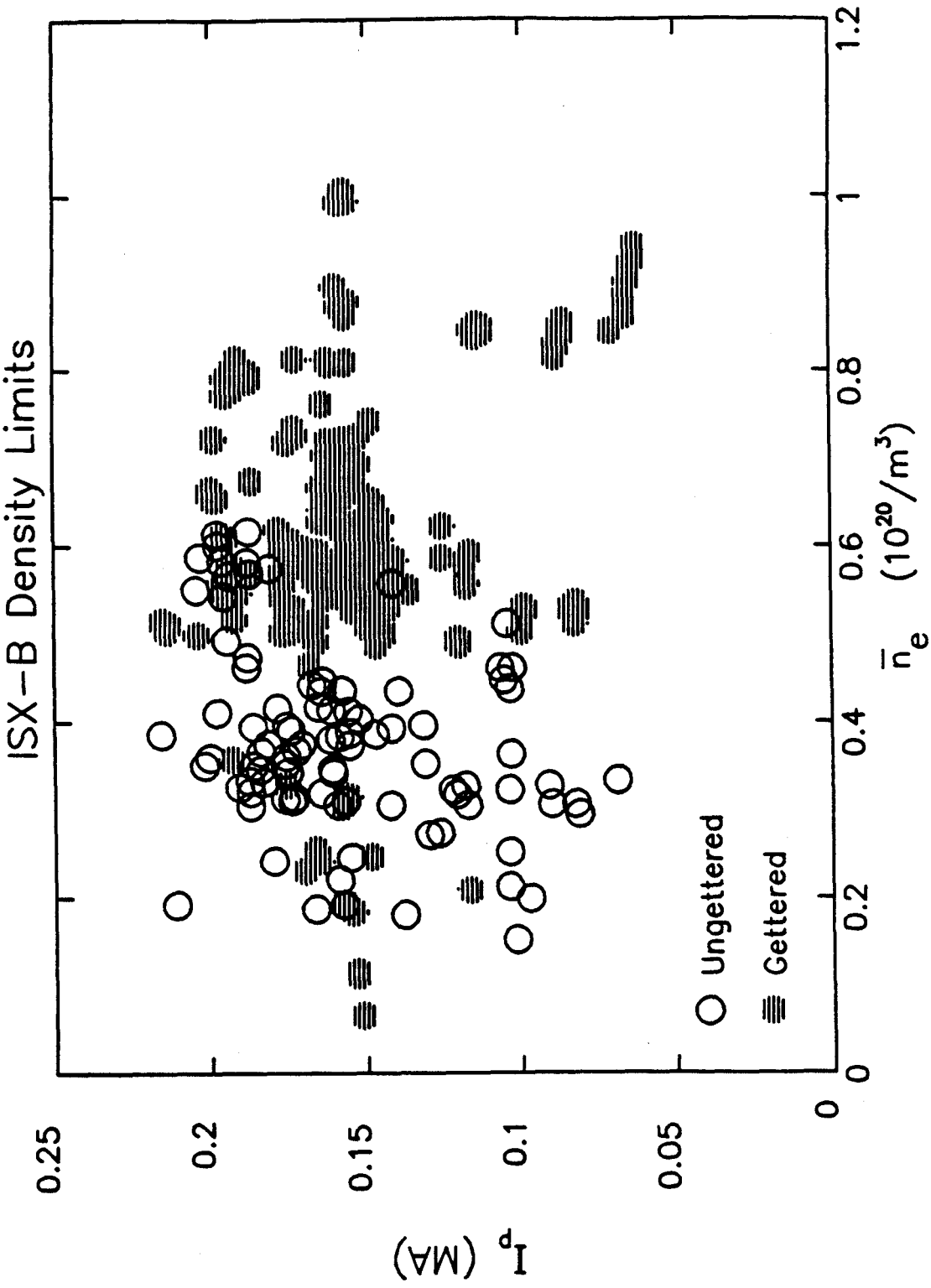


**Figure 10.** ISX-B data comparing gettered vs non-gettered discharges. While the highest densities are reached in gettered plasmas, then $n \sim I_p$ limit is essentially unaffected.

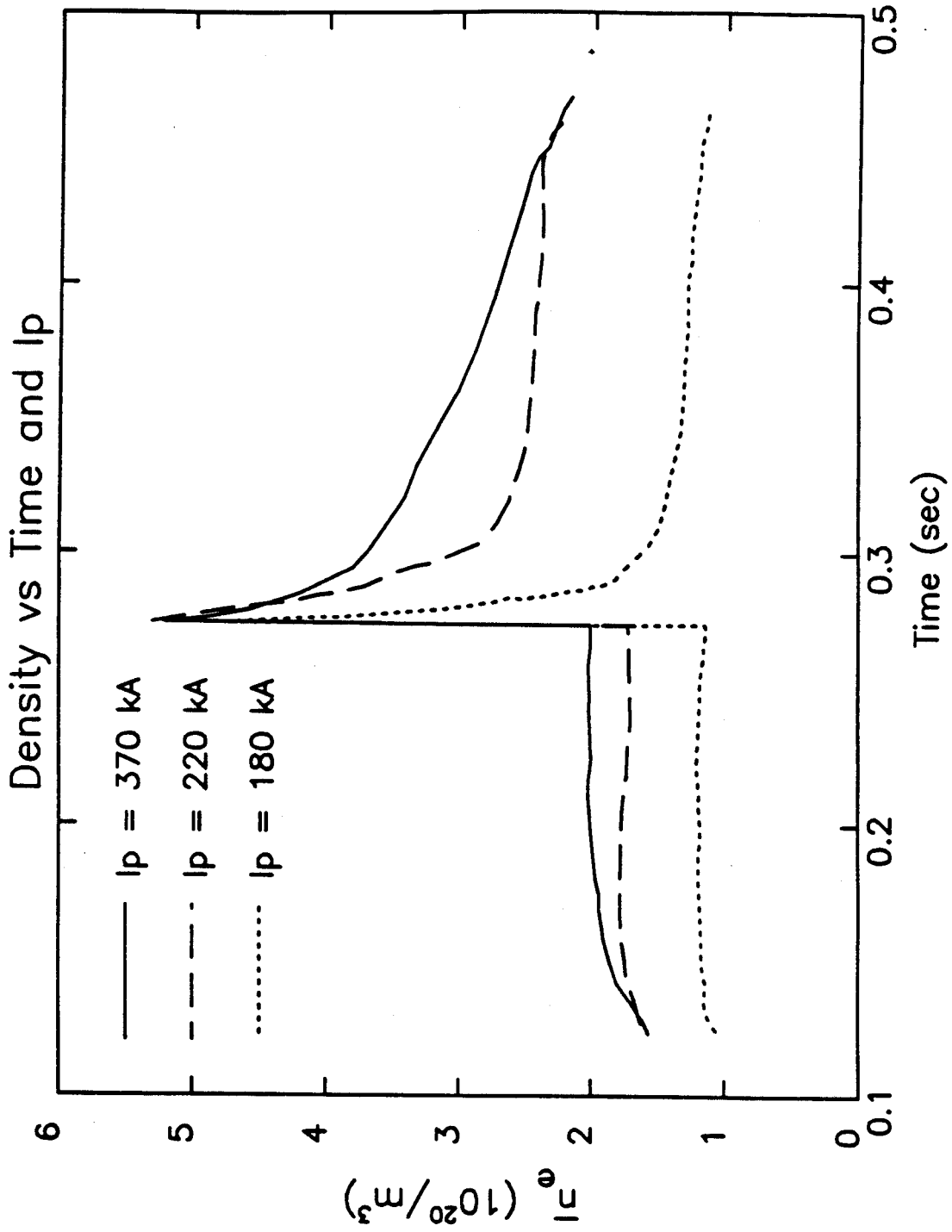


**Figure 11.** Density decay after injection of a single pellet for discharges with different plasma currents (Alcator C).

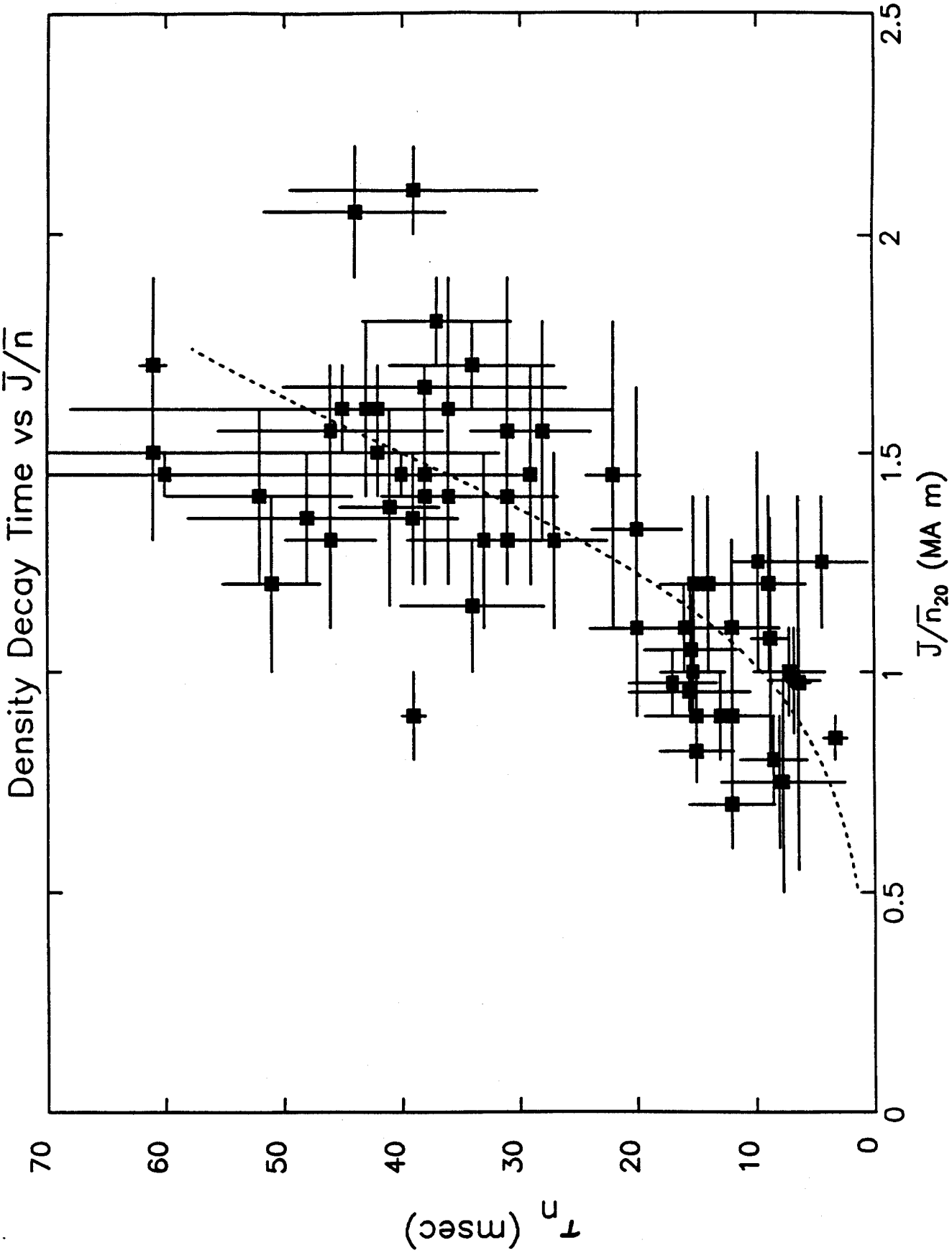


**Figure 12.** The density decay time (after pellet injection) plotted vs $J/n$. For Alcator, with $\kappa = 1$, the density limit is found at $J/n = 1$.

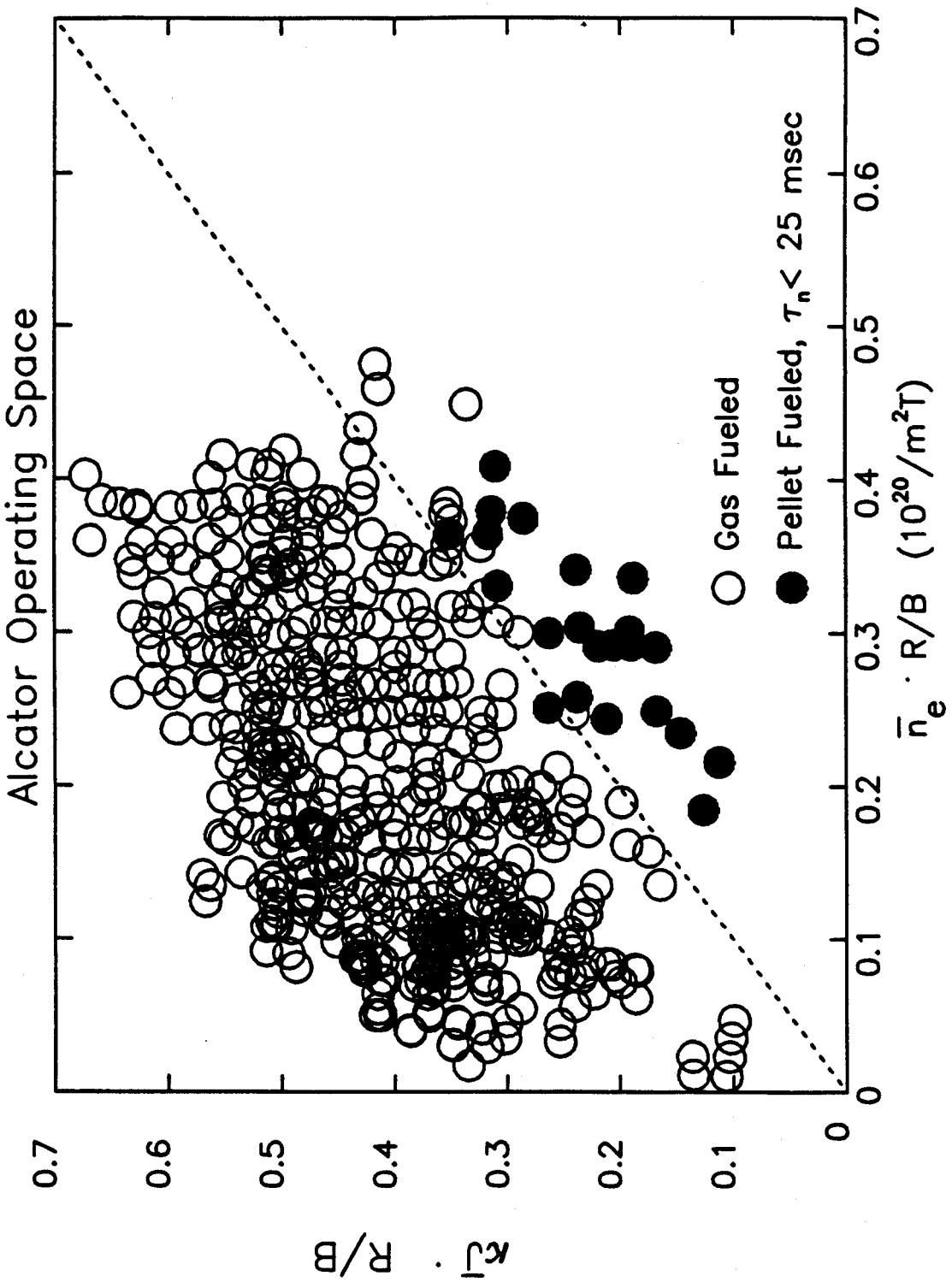


**Figure 13.** A DITE plot for Alcator C. Pellet fueled discharges with fast decay of density are plotted with solid points.